Dyes and Pigments 79 (2008) 224–235

Contents lists available at ScienceDirect

Dyes and Pigments

journal homepage: www.elsevier.com/locate/dyepig

Highly soluble perylene diimide and oligomeric diimide dyes combining perylene and hexa(ethylene glycol) units: Synthesis, characterization, optical and electrochemical properties

Jagadeesh B. Bodapati, Huriye Icil *

Department of Chemistry, Faculty of Arts and Science, Eastern Mediterranean University, Famagusta, N. Cyprus, Mersin 10, Turkey

ARTICLE INFO

Article history:
Received 4 December 2007
Received in revised form 6 February 2008
Accepted 9 February 2008
Available online 29 February 2008

Keywords:
Perylene polyimide
Oligomer
Solubility
Electrochemistry
Thermally stable
Color tunability

ABSTRACT

A novel, soluble, perylene oligomeric diimide dye, termed EOPPI was synthesized in high yield; for comparison, a small dye molecule, termed EOPDI, was also synthesized; both products readily dissolved in a wide range of organic solvents. The compounds were characterized using NMR, IR, MS, UV–vis, MS, GC–MS, HRMS, DSC, TGA, elemental analysis and cyclic voltammetry. The average molecular mass of EOPPI was 4460, its intrinsic viscosity was 0.3 dl g^{-1} in *m*-cresol at 20 °C. The band gap energy (E_g), LUMO and HOMO energy values were 2.25, −3.78 and −6.03 eV for the small dye molecule and 2.24, −3.85 and −6.09 eV for the oligomer, respectively. The temperatures at which the monomer and oligomer began to lose mass were 300 and 375 °C, respectively. The oligomer showed concentration-dependent color tunability.

1. Introduction

In the research for organic solar cells with high efficiency, the development of new materials offering optimized thermal and photochemical stabilities, optical, electrical, and structural properties plays an important role. Perylene diimides and polymers are attractive owing to their strong absorption and fluorescence, electroactive and photoactive properties, and excellent thermal, chemical and photochemical stability [1–5]. Unfortunately, they suffer from poor solubility and aggregation in common solvents and low solid-state fluorescence quantum efficiency which results from its self-quenching due to the high dye concentration within the thin film. The syntheses of various perylene polymers for better solubility have been reported in the literature [1–9]. Tian et al. reported the electrochemical and photophysical properties of a novel soluble and thermally stable fullerene dyad containing perylene [10]. Sundararajan et al. reported the nanoweb morphology exhibited by poly(dimethylsiloxane) end-capped with a perylene unit [11,12]. The syntheses of several liquid crystal (LC) perylene diimides and polymers have been studied [6–8]. The carrier transporting ability of dendron-functionalized perylene diimides for red luminescent materials is reported by Tian and co-workers [13]. Perylene monomers and polymers are efficient fluorophores for chemiluminescence and stable under peroxide oxidative condition [14–17]. Perylene polymers which show solid-state emission are very promising candidates for photovoltaic applications [18–21]. The power conversion efficiency of solar cells made from such materials is found to be moderate but encouraging [22–25]. Photoluminescent properties and hole and electron transporting ability were reported [26–28].

Furthermore, strong interactions at the excited state were determined between the perylene polymer containing 9,9-diphenylfluorene moieties and fullerene or carbon nanotubes [27]. The nanobelts fabricated from a perylene molecule showed linearly polarized emission and offered for orientation sensitive applications, such as polarized light-emitting diodes and flat panel display [29].

On the other hand, incorporation of flexible segments of different lengths into rigid perylene polymer backbones is an important way for obtaining flexible (coil-like) polymers for self-organization and obtains better solubility with variable photoluminescence properties [30–37]. Emission property is affected greatly from interactions between two or more chromophores. Self-organization might supply an efficient path for charge transporting. Hay et al. reported the synthesis of perylene-containing poly(imidoaryl ether) which was soluble, fluorescent and could be cast into flexible films [32]. π-Conjugated blocks of perylene bisimides are combined in polymers with polytetrahydrofuran blocks of varying molecular weight to obtain ordered conjugated polymers which showed

* Corresponding author. Tel.: +90 392 630 1085; fax: +90 392 630 2545.
E-mail address: huriye.icil@emu.edu.tr (H. Icil).

0143-7208/$ – see front matter © 2008 Elsevier Ltd. All rights reserved.
doi:10.1016/j.dyepig.2008.02.009

different aggregation in dichlorobenzene [32,33]. The self-organized, polymeric chromophore exhibits unstructured, long-lived, red-shifted "excimer-type" fluorescence [33].

Polymers with sequences of rigid hydrophobic perylenes and flexible hydrophilic tetra(ethylene glycol) were synthesized for studying folding and self-assembly which could play an important role in the future development of nanotechnology and biotechnology [34]. Wang et al. decided to employ oligo(ethylene glycol) as the flexible chain and use phosphoramidite chemistry to connect them in order to reach conjugated rigid sequences [33]. Lee et al. reported the polymer containing perylene and tri(ethylene oxide) moieties and the characteristic of the light-emitting electrochemical cell (LEC) based on it [34]. TGA measurements showed that the polymers consisting of alternating perylene bisimide chromophores and flexible oligo(ethylene glycol) start to decompose around 250–300 °C [32,34,35]. Perylene polymers which have anthracene moieties at the bay position showed longer fluorescence lifetime due to extending π-system in some degree [36]. Interestingly, modifying the molecular skeletons of the monomers or introducing new and more electron deficient units into the acceptor molecules, it is expected that more stable binding motifs may be generated [37].

In this work, we designed and synthesized a flexible–rigid–flexible perylene oligomer dye, perylene-3,4,9,10-tetracarboxylic acid-bis-(*N*,*N*'-bis 2-[2-(2-{2-[2-(2-hydroxy-ethoxy)-ethoxy]-ethoxy}-ethoxy)-ethoxy]-ethylpolyimide) (EOPPI) for exploring the emission properties which may show variation due to folding properties. In order to obtain a foldable oligomer, the planar perylene tetracarboxylic diimide unit is designed as the rigid hydrophobic chromophore and hexa(ethylene glycol) as the flexible hydrophilic spacer within the backbone. By using the flexible moiety, we were able to enhance the solubility also due to the decrease in rigidity. At the same time, a small dye molecule EOPDI has been synthesized as model compound for comparison. We investigated and compared the optical, thermal and electrochemical properties of the new oligomer and model compound in detail.

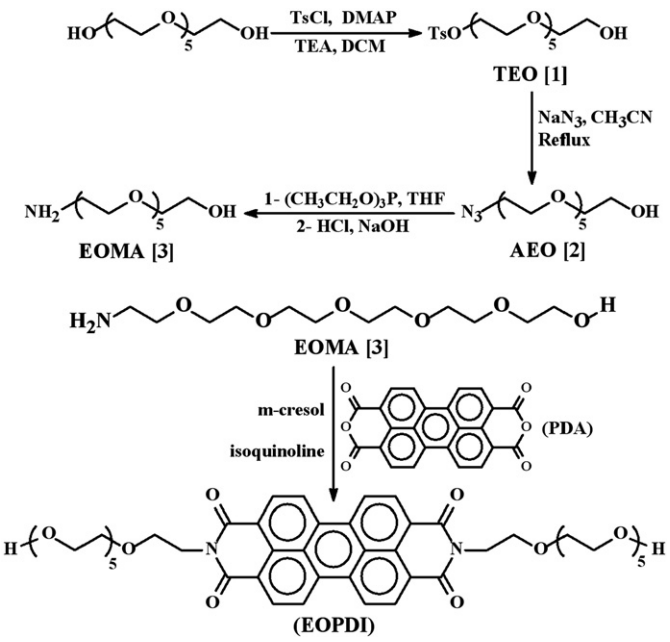

Scheme 1. Synthesis toward the monomeric model compound EOPDI.

2. Experimental

2.1. Chemicals and instruments

Commercially available reagents (Aldrich) and solvents (Aldrich) were used without further purification unless stated otherwise. The solvents chloroform ($CHCl_3$, CHL), dichloromethane (CH_2Cl_2, DCM) and methanol (CH_3OH) were obtained from Aldrich and purified by distillation. Organic solvent solutions were dried over sodium sulfate (Na_2SO_4) and evaporated on a rotary evaporator under reduced pressure. Column chromatography was performed on Merck silica gel 60 (0.063–0.20 mm or 0.04–0.063 mm). All reactions were monitored by thin layer chromatography (TLC) on Merck silica gel 60 F_{254} precoated aluminum plates, which were developed with UV light followed by spraying with acidic vanillin solution.

^1H (400 MHz) and ^{13}C NMR (100 MHz) spectra were recorded on a Bruker/XWIN spectrometer using tetramethyl silane (TMS) as an internal standard in deuterio dichloromethane (CD_2Cl_2) and deuterio chloroform ($CDCl_3$). Infrared spectra were obtained through KBr pellets using a Bruker IFS 66 Fourier transform FT-IR spectrophotometer. UV spectra in solutions were recorded with a Varian-Cary 100 spectrophotometer. UV spectra of solid state were measured in thin films using a Perkin–Elmer UV/VIS/NIR Lambda 19 spectrometer, equipped with solid accessories. Mass spectra were recorded with a Finnigan MAT 311A instrument at 70 eV ionization energy. Data were presented in *m*/*z* (%) values. Emission spectra were measured using a Varian-Cary Eclipse Fluorescence spectrophotometer. Elemental analyses were obtained from a Carlo-Erba-1106 C, H, N analyzer. TGA thermograms were recorded with a TG-MS: Simultane TG-DTA/DSC apparatus STA 449 Jupiter from Netzsch, equipped with Balzers Quadstar 422 V. The samples were heated at 10 K min^{-1} in oxygen. Thermal analyses were recorded using a DSC 820 Mettler Toledo instrument. The samples were heated at 10 K min^{-1} in nitrogen. Cyclic (CV) and square-wave voltammograms (SWV) in dichloromethane were performed using a three-electrode cell with a polished 2 mm glassy carbon as working and Pt as counter electrode; solutions were 10^{-4} M in electroactive material and 0.1 M in supporting electrolyte, tetrabutylammonium hexafluorophosphate (TBAPF6). Data were recorded on an EG & G PAR 273A computer-controlled

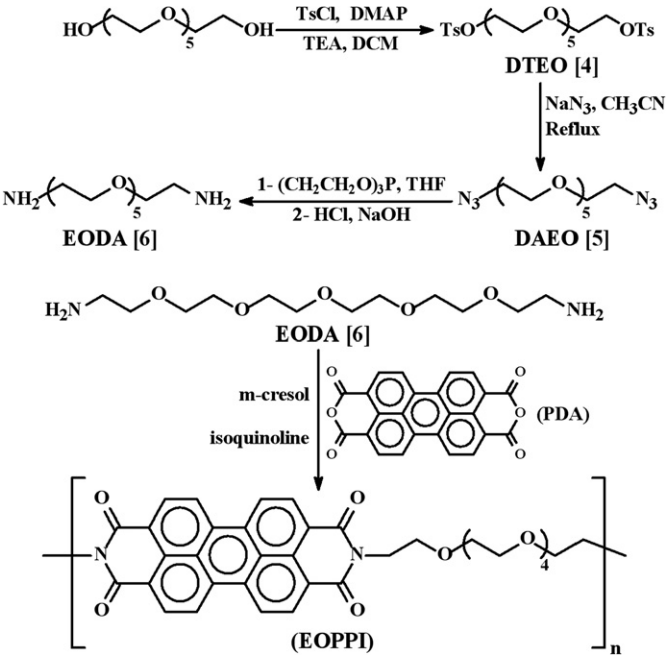

Scheme 2. Synthesis toward the oligomer EOPPI.

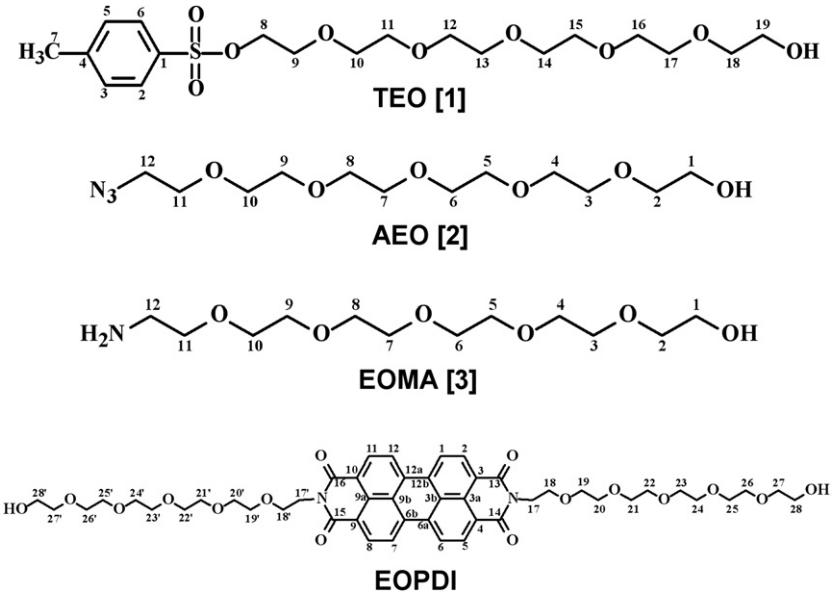

Scheme 3. The structures of synthesized compounds toward the monomeric model compound EOPDI with carbon numbering.

potentiostat. Ferrocene was used as an internal reference. All solutions in the cell were purged with argon before measurements. The scan rate of 25–1000 mV s^{-1} and the frequency of 60 Hz were employed for cyclic and square-wave voltammetries, respectively. Fluorescence lifetime measurements were performed by time correlated single photon counting technique (FLS920, from Edinburgh Instruments). The weight-average molecular weight (M_w) and number-average molecular weight (M_n) were determined by gel permeation chromatography (GPC) with a high performance liquid chromatography (HPLC) system from ThermoSeperationProducts using two columns (PSS-PFG, 7 μm 10^2 and 10^3 Å), with isocratic pump, autosampler, in combination with a detector Shodex R171. The samples were to run in hexafluoroisopropanol (HFIP) with 0.05 M potassiumtrifluoracetate (KTFAc) and calibrated with polymethylmethacrylate (12 narrow PMMA) standard at 23 °C. The oligomer was completely soluble in HFIP. The solution was filtered through a 1 μm filter unit and 50 μm was injected for the GPC measurement. Intrinsic viscosity was measured at 20 °C in *m*-cresol, using an Ubbelohde viscometer. The intrinsic viscosity value [η] was obtained by measuring specific viscosity $\eta_{sp} = \eta/\eta_o - 1$ and reduced viscosity $\eta_{red} = \eta_{sp}/c$ at five different concentrations, plotting η_{sp}/c vs. *c* and extrapolating to zero concentration.

2.2. Synthesis of model compound (EOPDI, Schemes 1 and 3) and oligomeric diimide dye (EOPPI, Schemes 2 and 4)

The reaction routes for the preparation of flexible–rigid–flexible monomeric model compound and oligomer are given in Schemes 1 and 2. EOPDI was synthesized by condensation of flexible amine, 2-[2-(2-{2-[2-(2-amino-ethoxy)-ethoxy]-ethoxy}-ethoxy)-ethoxy]-ethanol (EOMA [3]) with rigid perylene-3,4,9,10-tetracarboxylic dianhydride. Similarly, EOPPI was synthesized by one-step

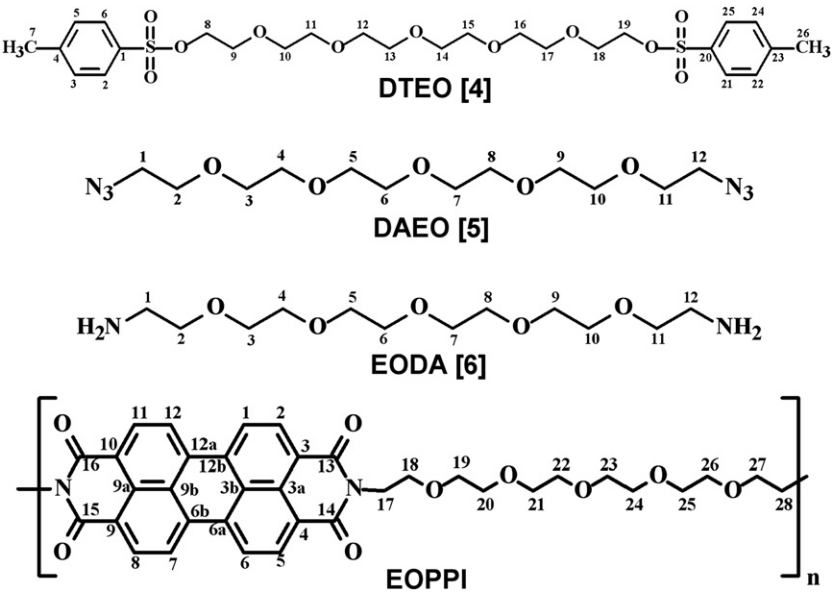

Scheme 4. The structures of synthesized compounds toward the oligomer EOPPI with carbon numbering.

Table 1
Solubility of EOPDI and EOPPI

Solubility[a]/color[a]		
Solvent	EOPDI	EOPPI
$CHCl_3$	(+ +) F brown	(+ +) F brown
TCE	(+ +) Brown	(+ +) Brown
THF	(− +) F yellow	(− +) F orange
CH_2Cl_2	(+ +) F orange	(+ +) F orange
Pyridine	(+ +) F pink	(+ +) F orange
Acetone	(− +) F yellow	(− +) F yellow
NMP	(+ +) Brown	(+ +) Brown
DMF	(+ +) F pink	(+ +) F pink
CH_3CN	(− +) F yellow	(− +) F yellow
DMSO	(+ +) Deep pink	(+ +) Cherry red
m-Cresol	(+ +) Deep pink	(+ +) Deep pink
CH_3COOH	(+ +) Pink	(+ +) Orange
CF_3COOH	(+ +) Deep pink	(+ +) Deep pink
CH_3OH	(− −)	(− −)
H_2SO_4	(+ +) Violet	(+ +) Deep violet

(+ +): Soluble at RT, (− +): Soluble on heating at 60 °C, (− −): insoluble.
[a] F: fluorescent, TCE: 1,1,2,2-tetrachloroethane, THF: tetrahydrofuran, NMP: *N*-methylpyrrolidinone, DMF: dimethylformamide, DMSO: dimethyl sulfoxide.

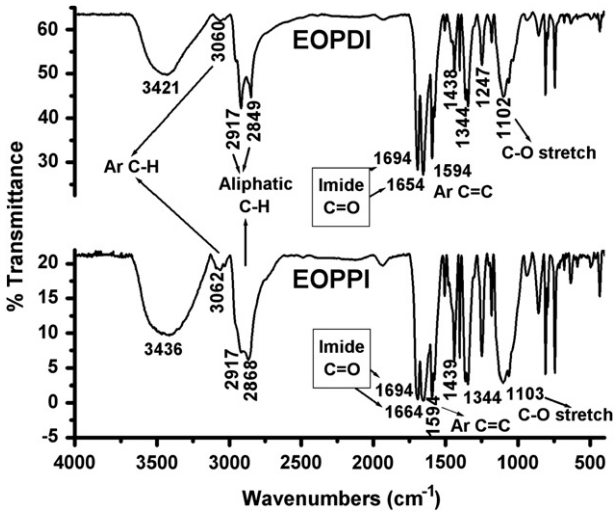

Fig. 2. FT-IR spectra of EOPDI and EOPPI.

polycondensation of flexible diamine, 2-[2-(2-{2-[2-(2-amino-ethoxy)-ethoxy]-ethoxy}-ethoxy)-ethoxy]-ethylamine (EODA [6]) with rigid perylene-3,4,9,10-tetracarboxylic dianhydride. For the model compound synthesis, we first activated one hydroxyl of hexa(ethylene glycol) by the action of tosylation, which yields the monotosylation product of hexa(ethylene glycol), toulene-4-sulfonic acid 2-[2-(2-{2-[2-(2-hydroxy-ethoxy)-ethoxy]-ethoxy}-ethoxy)-ethoxy]-ethyl ester (TEO [1]). Afterwards, the tosylate was replaced with an azido group to give 2-[2-(2-{2-[2-(2-azido-ethoxy)-ethoxy]-ethoxy}-ethoxy)-ethoxy]-ethanol (AEO [2]). Reduction of the azide AEO [2] yielded 2-[2-(2-{2-[2-(2-amino-ethoxy)-ethoxy]-ethoxy}-ethoxy)-ethoxy]-ethanol (EOMA [3]), which was condensed with perylene-3,4,9,10-tetracarboxylic dianhydride to yield the flexible–rigid–flexible model compound EOPDI. Similarly, for the oligomer synthesis, we activated both hydroxyls of hexa(ethylene glycol) by the action of tosylation, which yields the ditosylation product of hexa(ethylene glycol), 1-toulene-4-sulfonic acid 2-[2-(2-{2-[2-(2-toulene-4-sulfonic acid-ethoxy)-ethoxy]-ethoxy}-ethoxy)-ethoxy]-ethane (DTEO [4]). Then, the tosylates were replaced with azido groups to obtain 1-azido-2-[2-(2-{2-[2-(2-azido-ethoxy)-ethoxy]-ethoxy}-ethoxy)-ethoxy]-ethane (DAEO [5]). Finally, reduction of the azides DAEO [5] yielded 2-[2-(2-{2-[2-(2-amino-ethoxy)-ethoxy]-ethoxy}-ethoxy)-ethoxy]-ethylamine (EODA [6]), which was condensed with perylene-3,4,9,10-tetracarboxylic dianhydride to yield the flexible–rigid–flexible oligomer EOPPI.

2.2.1. Toulene-4-sulfonic acid 2-[2-(2-{2-[2-(2-hydroxy-ethoxy)-ethoxy]-ethoxy}-ethoxy)-ethoxy]-ethyl ester (TEO [1])

2-[2-(2-{2-[2-(2-hydroxy-ethoxy)-ethoxy]-ethoxy}-ethoxy)-ethoxy]-ethanol (3.00 g, 10.6 mmol), triethylamine (1.48 ml), 4-dimethylaminopyridine (0.016 g, 0.131 mmol) were dissolved in 80 ml of dichloromethane and cooled on an ice bath. A solution of 4-toulenesulfonyl chloride (0.506 g, 2.65 mmol) in 20 ml of DCM was added drop wisely over 2 h. The solution was stirred for an additional 5 h, washed with 5% aq. $NaHCO_3$ (100 ml), followed by aq. acetic acid buffer (0.2 M, pH = 4.5, 100 ml). The combined organic layers were dried over Na_2SO_4, and chromatographed (silica gel, 2% CH_3OH/CH_2Cl_2) to get the pure product TEO [1] as colorless oil (0.882 g, 76% yield). $R_f = 0.432$ (CH_2Cl_2: 2% CH_3OH).

^1H NMR (CD_2Cl_2, ppm): δ_H 7.79 (d, $J = 8.35$ Hz, 2Ar–H, H–C(2), H–C(6)), 7.38 (d, $J = 8.05$ Hz, 2Ar–H, H–C(3), H–C(5)), 4.14 (t, $J = 5$ Hz, $1CH_2$, H_2–C(8)), 3.66–3.55 (m, $11CH_2$, H_2–C(9)–H_2–C(19)), 2.57 (s, 1OH, HO–C(19)), 2.44 (s, $1CH_3$, C(7)). ^{13}C NMR (CD_2Cl_2, ppm): δ_C 145.44, 133.35, 130.24, 128.23, 72.94, 70.97, 70.88, 70.86, 70.84, 70.79, 70.75, 70.58, 70.39, 69.89, 68.95, 61.93, 21.72. FT-IR (KBr, cm^{-1}): ν 3415, 3063, 2880, 2590, 1940, 1640, 1597, 1453, 1359, 1293, 1249, 1174, 1104, 1012, 924, 819, 776, 664, 555. HRMS

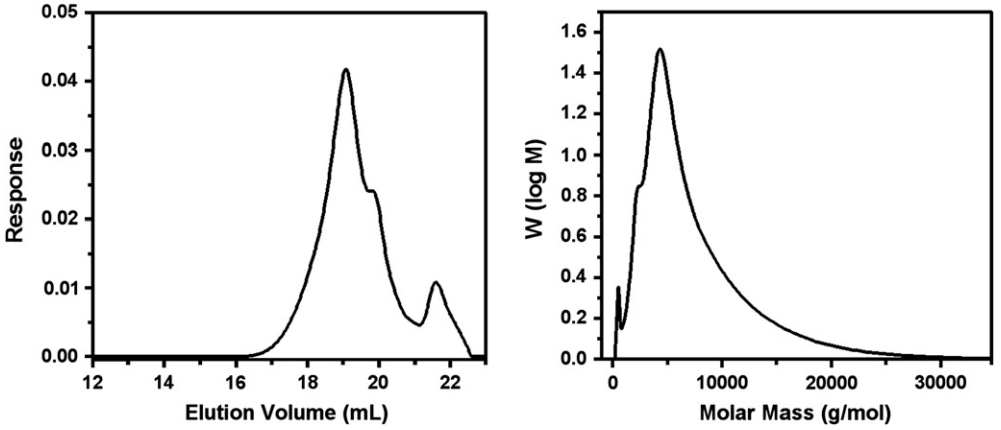

Fig. 1. GPC chromatograms of the oligomer EOPPI.

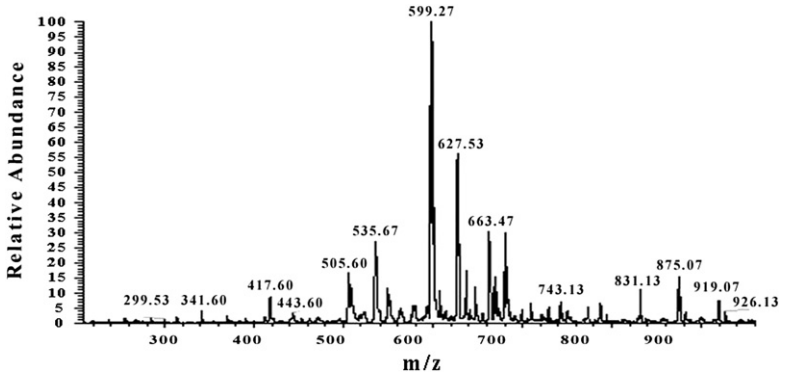

Fig. 3. Mass spectrum of EOPDI.

(chemical ionization (CI)): *m/z* 437.184 (437.184 calcd. for $C_{19}H_{32}O_9S$, $M^+ + H$).

2.2.2. 2-[2-(2-{2-[2-(2-Azido-ethoxy)-ethoxy]-ethoxy}-ethoxy)-ethoxy]-ethanol (AEO [2])

Toulene-4-sulfonic acid 2-[2-(2-{2-[2-(2-hydroxy-ethoxy)-ethoxy]-ethoxy}-ethoxy)-ethoxy]-ethyl ester, TEO [1] (0.8814 g, 2.02 mmol) and sodium azide (0.192 g, 2.95 mmol) were dissolved in 23 ml of acetonitrile and heated at reflux for 34 h. The solution was then cooled to room temperature, diluted with 20 ml of distilled water, and extracted with CH_2Cl_2 (3×50 ml). The total collected dichloromethane layers were dried over Na_2SO_4, and evaporated to yield AEO [2] as yellow oil (0.6 g, 97% yield). $R_f = 0.375$ (CH_2Cl_2: 2% CH_3OH).

^{1}H NMR (CD_2Cl_2, ppm): δ_H 3.67–3.63 (m, 10CH_2, H_2–C(1)–H_2–C(10)), 3.56 (t, $J = 5$ Hz, 1CH_2, C(11)), 3.38 (t, $J = 5.0$ Hz, 1CH_2, C(12)), 2.57 (s, OH, C(1)). ^{13}C NMR (CD_2Cl_2, ppm): δ_C 72.91, 70.96, 70.94, 70.89, 70.86, 70.84, 70.66, 70.24, 61.98, 51.18. FT-IR (KBr, cm^{-1}): ν 3410, 2875, 2520, 2104, 1941, 1644, 1454, 1348, 1290, 1250, 1109, 948, 886, 833, 641, 557. HRMS (electrospray ionization positive, ESI_{pos}): 330.163 (330.330 calcd. for $C_{12}H_{25}N_3O_6$, $M^+ + Na$). MS (GC–MS/GC–electron impact (EI), *m/z*): 279 ($M - 28$), 261, 248, 232, 218, 188, 163, 144, 133, 103, 89, 72, 59, 45.

2.2.3. 2-[2-(2-{2-[2-(2-Amino-ethoxy)-ethoxy]-ethoxy}-ethoxy)-ethoxy]-ethanol (EOMA [3])

2-[2-(2-{2-[2-(2-azido-ethoxy)-ethoxy]-ethoxy}-ethoxy)-ethoxy]-ethanol, AEO [2] (0.8236 g, 2.7 mmol) and triethyl phosphite (0.51 ml) were dissolved in 7 ml of tetrahydrofuran (THF) and heated at 70 °C for 20 h. The solution was cooled down to the room temperature and THF was evaporated to obtain intermediate product. The intermediate product was allowed to react with 40 ml of 12 M HCl and heated at 70 °C for 15 h. The solution pH was adjusted to 10 and extracted with CH_2Cl_2 (4×50 ml). The combined organic layer was dried over Na_2SO_4, and evaporated to yield EOMA [3] as greenish yellow oil (0.185 g, 25% yield). $R_f = 0.117$ (CH_2Cl_2: 2% CH_3OH).

^{1}H NMR ($CDCl_3$, ppm): δ_H 4.06–4.02 (m, 1CH_2, C(1)), 3.69–3.41 (m, 10CH_2, 1NH_2, H_2N–C(12), H_2–C(2)–H_2–C(11)), 3.31–3.29 (t, $J = 5.0$ Hz, 1CH_2, H_2–C(12)), 2.90 (s, OH, (1)). FT-IR (KBr, cm^{-1}): ν 3440, 2872, 2743, 2112, 1942, 1647, 1458, 1351, 1300, 1250, 1201, 1109, 947, 885, 833, 742, 662, 540. HRMS (CI): *m/z* 282.184 (282.191 calcd. for $C_{12}H_{27}NO_6$, $M^+ + H$).

2.2.4. N,N'-bis 2-[2-(2-{2-[2-(2-hydroxy-ethoxy)-ethoxy]-ethoxy}-ethoxy)-ethoxy]-ethyl-3,4,9,10-perylenebis(dicarboximide) (EOPDI)

Perylene-3,4,9,10-tetracarboxylic dianhydride (0.11 g, 0.28 mmol) and 2-[2-(2-{2-[2-(2-amino-ethoxy)-ethoxy]-ethoxy}-ethoxy)-ethoxy]-ethanol, EOMA [3] (0.18 g, 0.64 mmol) were heated in a carefully dried solvent mixture (60 ml *m*-cresol and 10 ml isoquinoline) under nitrogen atmosphere at 100 °C for 4 h, 120 °C for 6 h, 150 °C for 5 h and finally at 200 °C for 2 h. The solution was allowed to cool and poured into 100 ml methanol. The precipitate was filtered off and dried at 100 °C under vacuum. The product was treated with methanol in a Soxhlet apparatus for 1 day in order to get rid of the unreacted amine and high boiling solvents. EOPDI model compound was obtained as a brown powder (0.214 g, 83% yield).

^{1}H NMR (CD_2Cl_2, ppm): δ_H 7.78 (d, $J = 8.24$ Hz, 4Ar–H, H–C(1), H–C(6), H–C(7), H–C(12)), 7.37 (d, $J = 8.12$ Hz, 4Ar–H, H–C(2), H–C(5), H–C(8), H–C(11)), 4.13 (t, $J = 4.68$ Hz, 2CH_2, H_2–C(28), H_2–C(28')), 3.67–3.54 (m, 22CH_2, H_2–C(17)–H_2-C(27), H_2–C(17')–H_2–C(27')), 2.62 (s, 2OH, HO–C(28), HO–C(28')). ^{13}C NMR (CD_2Cl_2, ppm): δ_C 174.08, 145.43, 133.35, 130.22, 128.22, 72.89, 70.96, 70.87, 70.85, 70.84, 70.79, 70.74, 70.61, 69.87, 68.94, 61.92, 21.70. FT-IR (KBr, cm^{-1}): ν 3421, 3060, 2917, 2849, 1927, 1694, 1654, 1594, 1506, 1438, 1402, 1344, 1247, 1180, 1102, 936, 856, 809, 745, 433. UV–vis

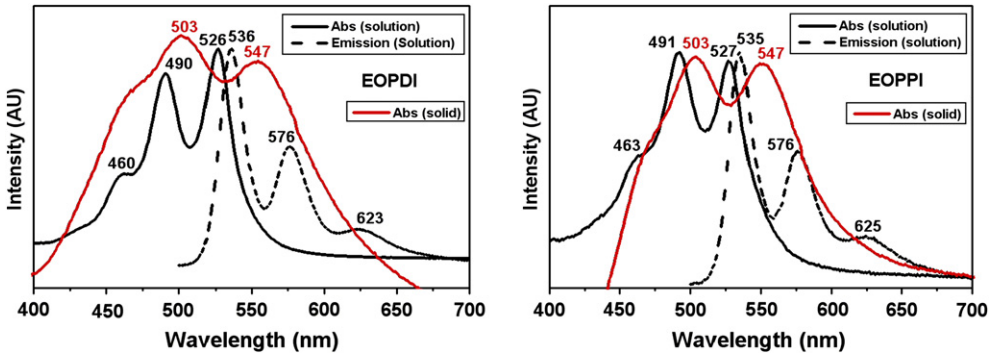

Fig. 4. Absorption (in solid state and chloroform at 10^{-5} M) and emission ($\lambda_{exc} = 485$ nm) spectra of EOPDI and EOPPI.

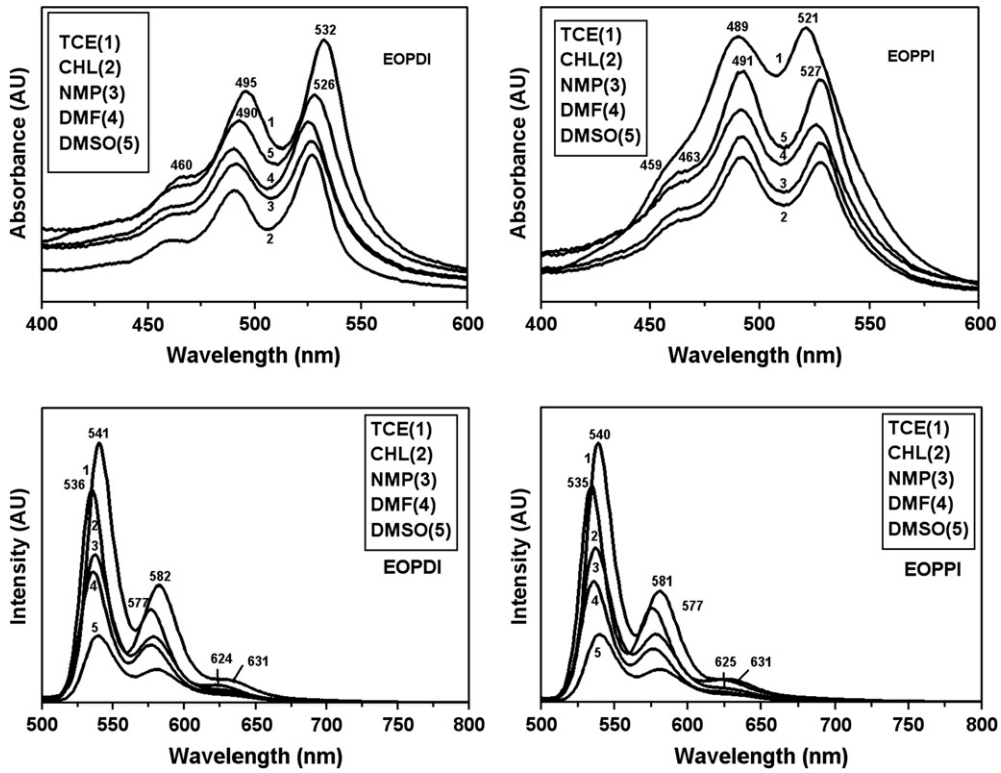

Fig. 5. UV–vis absorption and emission ($\lambda_{exc} = 485$ nm) spectra of EOPDI and EOPPI in various solvents (10^{-5} M, TCE: 1,1,2,2-tetrachloroethane, NMP: *N*-methylpyrrolidinone, DMF: dimethylformamide, DMSO: dimethyl sulfoxide).

($CHCl_3$), (λ_{max}, nm; (ε_{max}, $l\,mol^{-1}\,cm^{-1}$)): 460 (36,800), 490 (75,600), 526 (100,400). Fluorescence ($CHCl_3$), (λ_{max}, nm): 536, 576, 623, $\Phi_f = 0.49$. MS, (m/z) = 919.07 (M + 1), 875.07, 831.13, 743.13, 663.47, 627.53, 599.27, 535.67, 505.60, 443.60, 417.60. Anal. calcd. for $C_{48}H_{58}N_2O_{16}$ (M_w, 918.4): C, 62.732%; H, 6.362%; N, 3.049%. Found: C, 63.44%; H, 6.89%; N, 3.42%.

2.2.5. 1-Toulene-4-sulfonic acid 2-[2-(2-{2-[2-(2-toulene-4-sulfonic acid-ethoxy)-ethoxy]-ethoxy}-ethoxy)-ethoxy]-ethane (DTEO [4])

2-[2-(2-{2-[2-(2-hydroxy-ethoxy)-ethoxy]-ethoxy}-ethoxy)-ethoxy]-ethanol (1.50 g, 5.31 mmol), triethylamine (2.6 ml), 4-dimethylaminopyridine (0.016 g, 0.131 mmol) were dissolved in 40 ml of CH_2Cl_2 and cooled on an ice bath. A solution of 4-toulene-sulfonyl chloride (3.33 g, 17.5 mmol) in 20 ml of dichloromethane was added drop wisely over 2 h. Similar purification procedures are followed as stated in the synthesis of TEO [1] to obtain the pure product DTEO [4] as yellowish oil (2.8 g, 89% yield). $R_f = 0.7285$ (CH_2Cl_2: 2% CH_3OH).

^{1}H NMR (CD_2Cl_2, ppm): δ_H 7.78 (d, $J = 8.24$ Hz, 4Ar–H, H–C(2), H–C(6), H–C(21), H–C(25)), 7.37 (d, $J = 7.96$ Hz, 4Ar–H, H–C(3), H–C(5), H–C(22), H–C(24)), 4.12 (t, $J = 4.68$ Hz, $2CH_2$, H_2–C(8), H_2–C(19)), 3.64 (t, $J = 4.70$ Hz, $2CH_2$, H_2–C(9), H_2–C(18)), 3.55 (m, $8CH_2$, H_2–C(10)–H_2–C(17)) 2.44 (s, $2CH_3$, H_3–C(7), H_3–C(26)). ^{13}C NMR (CD_2Cl_2, ppm): δ_C 145.44, 133.35, 130.24, 128.23, 71.00, 70.89, 70.83, 70.75, 69.86, 68.95, 21.72. FT-IR (KBr, cm^{-1}): ν 3518, 3057, 2875, 1931, 1597, 1495, 1452, 1364, 1292, 1247, 1184, 1136, 1100, 1017, 921, 817, 776, 664, 559. HRMS (CI): m/z 591.184 (591.185 calcd. for $C_{26}H_{38}S_2O_{11}$, $M^+ + H$).

Table 2
Fluorescence quantum yield (Φ_f) data in different solvents

Fluorescence quantum yield, Φ_f		
Solvent[a]	EOPDI	EOPPI
TCE	0.28	0.31
$CHCl_3$	0.49	0.47
NMP	0.27	0.38
DMF	0.33	0.55
DMSO	0.07	0.12

[a] TCE: 1,1,2,2-tetrachloroethane, NMP: *N*-methylpyrrolidinone, DMF: dimethylformamide, DMSO: dimethyl sulfoxide.

2.2.6. 1-Azido-2-[2-(2-{2-[2-(2-azido-ethoxy)-ethoxy]-ethoxy}-ethoxy)-ethoxy]-ethane (DAEO [5])

1-Toulene-4-sulfonic acid 2-[2-(2-{2-[2-(2-toulene-4-sulfonic acid-ethoxy)-ethoxy]-ethoxy}-ethoxy)-ethoxy]-ethane (DTEO [4]) (1.1 g, 1.86 mmol) and sodium azide (0.32 g, 4.92 mmol) were dissolved in 35 ml of acetonitrile and heated at reflux 30 h. The solution was then cooled to room temperature, diluted with 20 ml of distilled water, and extracted with CH_2Cl_2 (3×50 ml). The total collected dichloromethane layers were dried over Na_2SO_4, and evaporated to yield DAEO [5] as yellow oil (0.61 g, 99% yield). $R_f = 0.7285$ (CH_2Cl_2: 2% CH_3OH).

^{1}H NMR (CD_2Cl_2, ppm): δ_H 3.66–3.59 (m, $8CH_2$, H_2–C(3)–H_2–C(10)), 3.37 (t, $J = 5.02$ Hz, $4CH_2$, H_2–C(1), H_2–C(12), H_2–C(2), H_2–C(11)). ^{13}C NMR (CD_2Cl_2, ppm): δ_C 70.97, 70.96, 70.87, 70.23, 51.16. FT-IR (KBr, cm^{-1}): ν 3507, 2869, 2741, 2528, 2104, 1732, 1634, 1451, 1347, 1301, 1124, 1037, 993, 941, 852, 664, 555, 505. HRMS (ESI_{pos}): 355.170 (355.346 calcd. for $C_{12}H_{24}N_6O_5$, $M^+ + Na$). MS (GC–MS/GC–EI, m/z): 304 (M − 28), 259, 245, 215, 188, 174, 158, 144, 130, 114, 87, 72, 56, 45.

2.2.7. 2-[2-(2-{2-[2-(2-amino-ethoxy)-ethoxy]-ethoxy}-ethoxy)-ethoxy]-ethylamine (EODA [6])

1-Azido-2-[2-(2-{2-[2-(2-azido-ethoxy)-ethoxy]-ethoxy}-ethoxy)-ethoxy]-ethane (DAEO [5]) (1.0531 g, 3.17 mmol) and triethyl phosphite (1.2 ml) were dissolved in 10 ml of tetrahydrofuran and heated at 70 °C for 20 h. Similar procedures are followed as stated

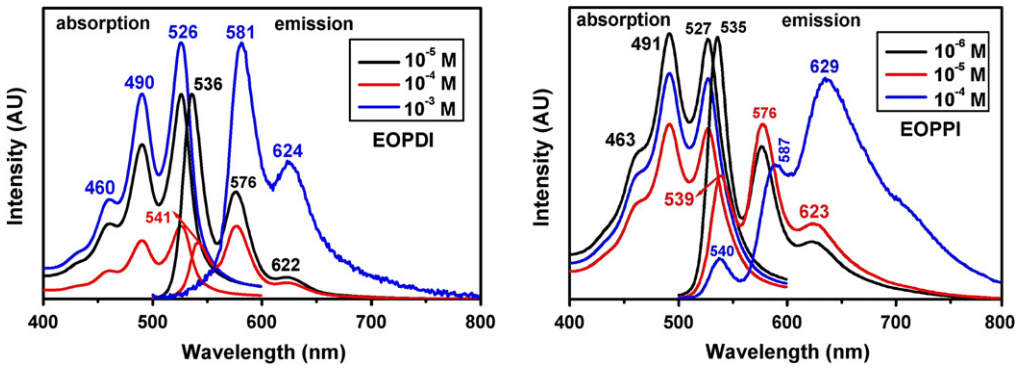

Fig. 6. Effect of concentration on the UV–vis and emission ($\lambda_{exc} = 485$ nm) spectra of EOPDI and EOPPI in chloroform.

in the synthesis of EOMA [3] to yield EODA [6] as greenish yellow oil (0.50 g, 56% yield). $R_f = 0.109$ (CH_2Cl_2: 2% CH_3OH).

^{1}H NMR (CD_2Cl_2, ppm): δ_H 4.60 (s, 2NH_2, H_2N–C(1), H_2N–C(12)), 3.78–3.42 (m, 8CH_2, H_2–C(3)–H_2–C(10)), 3.13 (m, 2CH_2, H_2–C(2), H_2–C(11)), 2.77 (s, 2CH_2, H_2–C(1), H_2–C(12)). ^{13}C NMR (CD_2Cl_2, ppm): δ_C 70.53, 69.73, 69.59, 69.51, 69.48, 69.21, 40.00. FT-IR (KBr, cm^{-1}): ν 3475, 2871, 2748, 2119, 1942, 1646, 1457, 1350, 1301, 1250, 1200, 1114, 947, 884, 833, 662, 573. MS (GC–MS/GC–EI, *m*/*z*): 279 (M − 1), 261, 248, 232, 218, 195, 176, 163, 144, 133, 119, 103, 89, 72, 59, 45.

*2.2.8. Perylene-3,4,9,10-tetracarboxylic acid-bis-(*N,N'*-bis 2-[2-(2-{2-[2-(2-hydroxy-ethoxy)-ethoxy]-ethoxy}-ethoxy)-ethoxy]-ethylpolyimide) (EOPPI)*

Perylene-3,4,9,10-tetracarboxylic dianhydride (1.212 g, 3.09 mmol) and 2-[2-(2-{2-[2-(2-amino-ethoxy)-ethoxy]-ethoxy}-ethoxy)-ethoxy]-ethylamine (EODA [6]) (0.8668 g, 3.09 mmol) were heated in a carefully dried solvent mixture (60 ml *m*-cresol and 10 ml isoquinoline) under nitrogen atmosphere at 80 °C for 3 h, at 120 °C for 4 h, at 160 °C for 5 h and finally at 200 °C for 10 h. The reaction water was collected in the Dean–Stark trap. The solution was allowed to cool and was poured into 300 ml methanol. The precipitate was filtered off and dried at 100 °C under vacuum. The crude product was treated with methanol in a Soxhlet apparatus for 2 days in order to get rid of the unreacted amine and high boiling solvents. Finally, the product was purified by crystallization from chloroform/methanol to obtain the oligomer as a black, shining powder (1.38 g, 70% yield).

^{1}H NMR ($CDCl_3$, ppm): δ_H 8.56 (br s, 4Ar–H, H–C(1), H–C(6), H–C(7), H–C(12)), 8.31 (br s, 4Ar–H, H–C(2), H–C(5), H–C(8), H–C(11)), 4.50–3.74 (m, 12CH_2, H_2–C(17)–H_2–C(28)). ^{13}C NMR ($CDCl_3$, ppm): δ_C 164.24, 134.59, 132.25, 124.82, 121.94, 77.41, 77.30, 77.09, 76.78, 70.43, 69.79, 68.44, 68.18, 66.54, 39.64, 28.55. FT-IR (KBr, cm^{-1}): ν 3436, 3062, 2917, 2868, 1934, 1694, 1664, 1594, 1506, 1439, 1409, 1339, 1247, 1180, 1103, 937, 857, 809, 744, 634, 496, 433. UV–vis ($CHCl_3$), (λ_{max}, nm): 463 (83,450), 491 (112,600), 527 (150,000). Fluorescence ($CHCl_3$), (λ_{max}, nm): 535, 576, 625, $\Phi_f = 0.47$. Anal. calcd. for $(C_{36}H_{32}N_2O_9)_n$, ($(M_w)_n$, 636.21): C, 67.91%; H, 5.07%; N, 4.40%. Found: C, 67.50%; H, 4.45%; N, 4.04%.

3. Results and discussion

3.1. Synthesis and characterization of perylene diimide and oligomeric diimide dyes

The synthetic route of monomeric model compound EOPDI and oligomer EOPPI are shown in Schemes 1 and 2. The amine EOMA and diamine EODA were successfully synthesized via three different steps. The synthesized products (Schemes 3 and 4) were characterized through the data from NMR, IR, MS, UV–vis, MS, GC–MS, HRMS, DSC, TGA, CV and elemental analysis. These characterizations confirmed the formation of all the compounds (Schemes 1 and 2).

Table 1 lists the solubility properties of the model compound and oligomer. The solubility was enhanced by the high flexibility of hexa(ethylene glycol) moiety. EOPPI showed higher solubility which is explained by the higher number of flexible hydrophilic spacers within the backbone. Both model compound and oligomer were readily soluble in various organic solvents such as $CHCl_3$, *N*-methylpyrrolidinone (NMP), dimethylformamide (DMF) and dimethyl sulfoxide (DMSO). However, they were insoluble in most polar protic solvents such as methanol and ethanol.

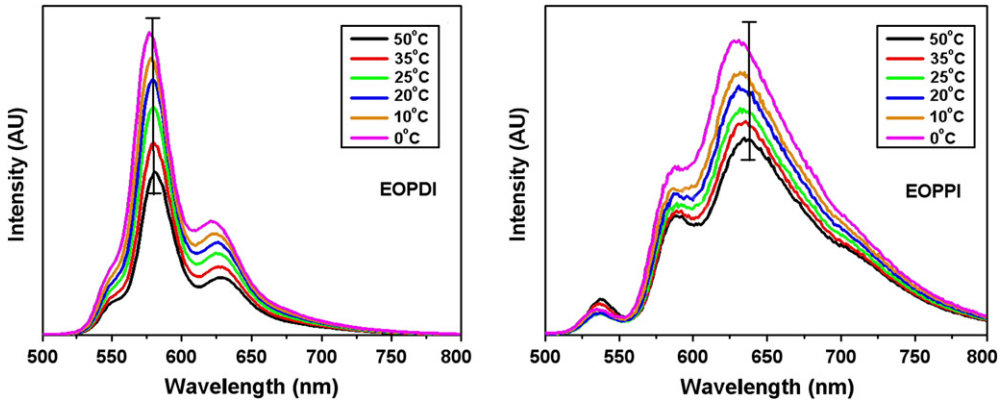

Fig. 7. Effect of temperature on emission ($\lambda_{exc} = 485$ nm) spectra of EOPDI and EOPPI in chloroform solution (1×10^{-3} M).

Table 3
Maximum absorption wavelengths λ_{max} (nm), extinction coefficients ε_{max} ($l\,mol^{-1}\,cm^{-1}$), oscillator strength f, fluorescence quantum yields Φ_f ($\lambda_{exc} = 485$ nm), radiative lifetimes τ_0 (ns), fluorescence lifetimes τ_f (ns), fluorescence rate constants k_f (sec^{-1}), rate constant of radiationless deactivation k_d (sec^{-1}) and singlet energy E_s ($kcal\,mol^{-1}$) data of EOPDI and EOPPI

	λ_{max}	ε_{max}	f	Φ_f	τ_0	τ_f[a]	k_f	k_d	E_s
EOPDI	526	100,400	0.41	0.49	10.1	4.95 (3.9)	9.9×10^7	1.0×10^8	54.4
EOPPI	527	150,000	0.77	0.47	5.46	2.57 (4.1)	1.8×10^8	2.0×10^8	54.3

[a] Experimental values are given in parenthesis.

GPC measurement was recorded in HFIP solution. The average molecular weight (M_w) of the oligomer was estimated about 4460 with a broad distribution (polydispersity ≅ 2.33) as expected from a polycondensation reaction (Fig. 1). Such moderate polydispersity was probably due to the side reactions upon extension. The oligomer has about seven monomer units. Intrinsic viscosity was measured as 0.3 $dl\,g^{-1}$ in *m*-cresol using an Ubbelohde suspended level viscometer at 20 °C. The measured intrinsic viscosity of the oligomer was in good agreement with the GPC data.

The IR spectra of all compounds were consistent with their chemical structures. As shown in Fig. 2, the IR spectrum of EOPDI exhibited characteristic absorption bands at 3060 (aromatic C–H stretch); 2917 and 2849 (aliphatic C–H stretch); 1694, 1654 (imide C=O stretch); 1594 (conjugated C=C stretch); 1344 (C–N stretch); 1102 (CH_2–O stretch); 809 and 745 (C–H bend) cm^{-1}. IR spectrum of the oligomer EOPPI showed similar but broader absorption bands with EOPDI, at 3062 (aromatic C–H stretch); 2917 and 2868 (aliphatic C–H stretch); 1694, 1664 (imide C=O stretch); 1594 (conjugated C=C stretch); 1339 (C–N stretch); 1103 (CH_2–O stretch); 809 and 744 (C–H bend) cm^{-1}. The comparison of the oligomer IR spectrum with that of monomeric model compound showed a drastic increase in intensity of the aliphatic C–H and imide C=O stretching bands at 2917–2868 and 1694–1654 cm^{-1}, respectively.

The MS, GC–MS, HRMS and elemental analysis results have confirmed the structures of AEO [2], DAEO [5], EODA [6] and EOPDI. The mass spectrum of the EOPDI (Fig. 3) showed the corresponding molecular ion peak at 919.07 *m*/*e* (M + 1). Results of elemental analyses and HRMS are in good agreement with the calculated values. Results of ^1H and ^{13}C NMR analysis are correlated very well with the calculated values based on chemical structures of the products (Schemes 3 and 4).

3.2. Optical properties

The absorption and emission spectra of EOPDI and EOPPI in solution (10^{-5} M) and their absorption spectra in solid state are shown in Figs. 4 and 5. Their respective maxima and fluorescence quantum yields are listed in Table 2. Fig. 5 shows the UV–vis absorption and emission ($\lambda_{exc} = 485$ nm) spectra of EOPDI and EOPPI in various solvents. The UV spectra of EOPDI (460, 490 and 526) and EOPPI (463, 491 and 527) were very similar. The emission band and Stoke shift values in CHL, NMP, DMF and DMSO were 536, 577, 624 and 10 nm for the model compound; and 535, 577, 625 and 8 nm for the oligomer, respectively. Interestingly, EOPDI showed a red shifted (460, 495 and 532 nm) and EOPPI blue shifted absorption peaks (459, 489 and 521 nm) in 1,1,2,2-tetrachloroethane (TCE). Meanwhile, both EOPDI and EOPPI showed red-shifted emission peaks at around 541, 582 and 631 nm in TCE. The absorption spectra of solid state were very different for the model compound and oligomer comparing to their solution absorption spectra in terms of the spectral shapes (absorption up to 650 nm) and peak positions (Fig. 4, 0 → 0 absorption bands were red shifted by about 20 nm). This is most likely due to intermolecular π interaction in the solid state. The solid-state emission of EOPDI and EOPPI could not be taken in all attempts due to the weak emission intensity. This was attributed to the self-quenching as a result of efficient energy transfer at solid state.

The emission spectra of EOPDI and EOPPI were taken at $\lambda_{exc} = 485$ nm and the relative fluorescence quantum yields were determined in various solvents using *N*,*N*′-didodecyl-3,4,9,10-perylenebis (dicarboximide) in chloroform as standard. The fluorescence quantum yields of compounds are measured and given in Table 2. The low fluorescence quantum yields in various solvents are attributed to the re-absorption of emitted photons and the self-quenching due to the intra and intermolecular interactions.

As shown in Fig. 6, at three different concentrations the intensities of the absorption bands decreased from 0 → 0 to 0 → 2. EOPDI has dominant emission at 536 nm (0 → 0), 576 nm (0 → 1) and 622 nm (0 → 2) when the concentration was 1×10^{-5} M. As a result of reciprocal transitions, the fluorescence spectrum exhibited mirror symmetry for all the absorption bands at this concentration. After a 10-fold increase in EOPDI concentration, the 0 → 0 emission band intensity at 541 nm reduced comparing to the intensity of (0 → 1) emission band at 576 nm. After a 100-fold increase in concentration, the 0 → 0 emission band diminished and the other peaks are observed at 581 nm (0 → 1) and at 624 nm (0 → 2). The UV absorption spectrum of the oligomer revealed clear differences. Notice that the 0 → 1 transition intensity is higher than that for 0 → 0 transition at 1×10^{-6}, 1×10^{-5} and 1×10^{-4} M concentrations for the oligomer. Meanwhile, the reciprocal transitions couldn't be obtained even at 1×10^{-6} M concentration. At 1×10^{-6} M EOPPI concentration, the dominant emissions are detected at 535 nm (0 → 0), 576 nm (0 → 1) and 623 nm (0 → 2). After a 10-fold increase in EOPPI concentration, the 0 → 0 emission

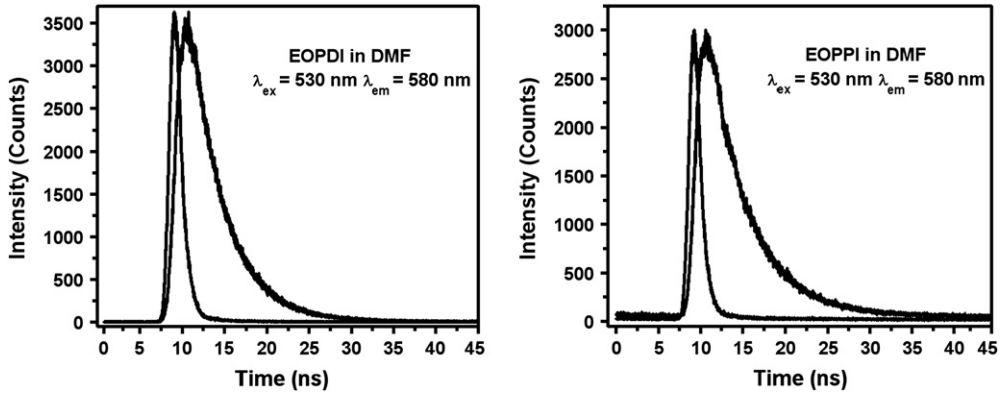

Fig. 8. Fluorescence decay curves of EOPDI and EOPPI in DMF (10^{-5} M, $\lambda_{exc} = 530$ nm and $\lambda_{em} = 580$ nm).

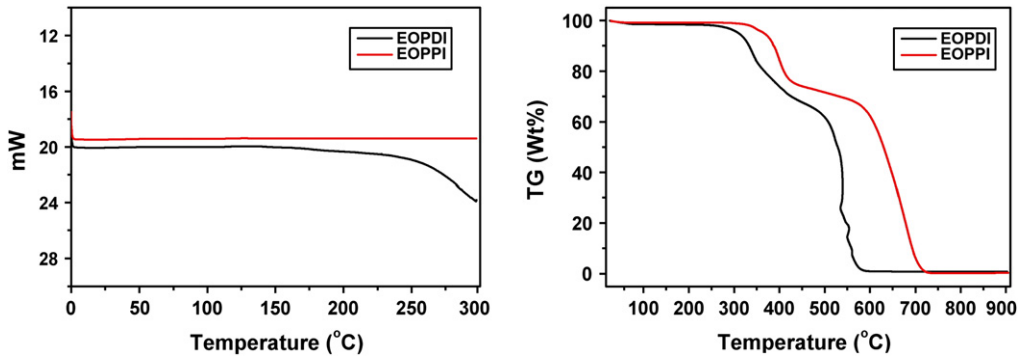

Fig. 9. DSC thermograms and thermogravimetric analysis (TGA) curves of EOPDI and EOPPI at a heating rate of 10 K min^{-1} under nitrogen and oxygen, respectively.

band intensity at 540 nm reduced comparing to the intensity of (0 → 1) emission band at 576 nm. The reasons for the decrease in 0 → 0 emission bands were related to the overlap between the absorption and emission spectra of compounds which could lead to re-absorption of the emitted photons by ground state and to the probable intra and intermolecular interactions. After a 100-fold increase in concentration, the 0 → 0 emission band diminished, the emission band intensity at 587 nm (0 → 1) reduced while the emission at 629 nm (0 → 2) increases significantly. The model compound net emission is at 581 nm at 1×10^{-3} M concentration. However, the oligomer net emission is enhanced and observed at 629 nm at lower concentration (1×10^{-4} M) than monomeric model compound. The oligomer emits green, yellow and red light at 1×10^{-6}, 1×10^{-5} and 1×10^{-4} M concentrations, respectively. It is noteworthy that the observed concentration-dependent emission tunability will remain a challenge in photonic applications. Wang et al. have reported similar tunability and attributed this result to the existence of folded polymers, which leads to the emission of different colors as the folded chromophoric oligomers become larger [33].

Fig. 7 shows the fluorescence properties of EOPDI and EOPPI upon heating. The emission maxima are blue shifted and decreased in emission intensity with increasing temperature. This optical change could be related to the conformational transition of the conjugated backbone and to aggregation. Oligomer showed higher blue shift due to its longer backbone.

This property is in agreement with the literature data [31,32]. Rene et al. have reported the self-organized three different perylene polymers, consisting of alternating segments of perylene bisimide chromophores and polyhydrofuran of different average lengths. They have explained the importance of the secondary carbon atoms next to nitrogen atoms, which force the alkyl chains out of the plane of the molecule and, thereby, hamper to face-to-face π–π stacking of the perylene bisimides [33]. Consequently, the lack of this secondary carbon atom causes aggregation in different extent for perylene monomers and polymers due to face-to-face π–π stacking.

Maximum absorption wavelengths (λ_{max} in nm, $CHCl_3$), extinction coefficients (ε_{max}, $CHCl_3$), oscillator strengths *f*, fluorescence quantum yields (Φ_f, $CHCl_3$), radiative lifetimes τ_0 (ns), fluorescence lifetimes τ_f (ns), fluorescence rate constants k_f, rate constant of radiationless deactivation k_d and singlet energies E_s (kcal mol^{-1}) data of all the compounds in chloroform, are given in Table 3. Fluorescence lifetimes of the compounds were measured in argon-saturated solutions.

The theoretical radiative lifetimes τ_0 were calculated according to the formula: $\tau_0 = 3.5 \times 10^8/\nu^2_{max}\varepsilon_{max}\Delta\nu_{1/2}$, where ν_{max} stands for the wavenumber in cm^{-1}, ε_{max} for the molar extinction coefficient at the selected absorption wavelength and $\Delta\nu_{1/2}$ indicates the half-width of the selected absorption in units of cm^{-1} [23]. Fluorescence lifetimes were calculated from $\tau_f = \tau_0 Q_f$ and the rates of fluorescence from $k_f = 1/\tau_0$ (Table 3). The technique of time correlated single photon counting was used to record fluorescence lifetimes of the compounds. The decay curves were multi-exponential and analysed by using the standard method of iterative reconvolution and non-linear least square fitting method (Fig. 8). The quality of

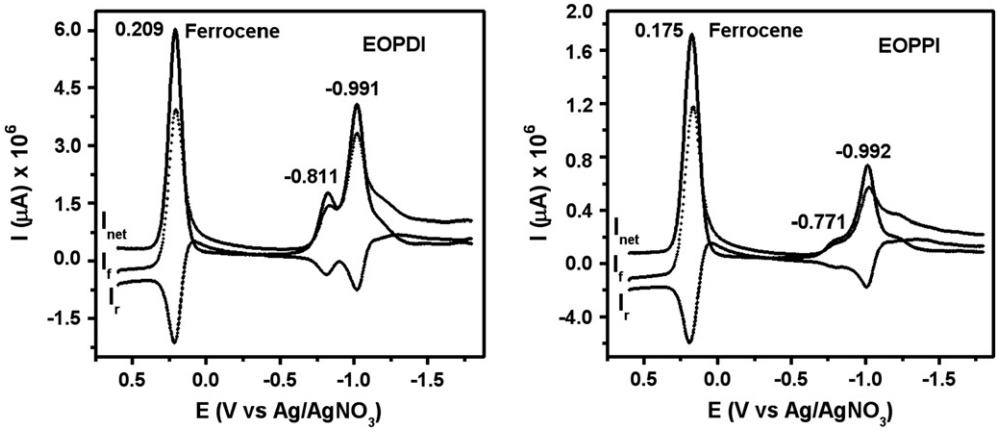

Fig. 10. Square-wave voltammograms (I_f: forward current, I_r: reverse current, I_{net}: net current, $I_{net} = I_f - I_r$) of EOPDI, EOPPI and ferrocene (in CH_2Cl_2/supporting electrolyte: $TBAPF_6$, frequency: 60 Hz) at 25 °C.

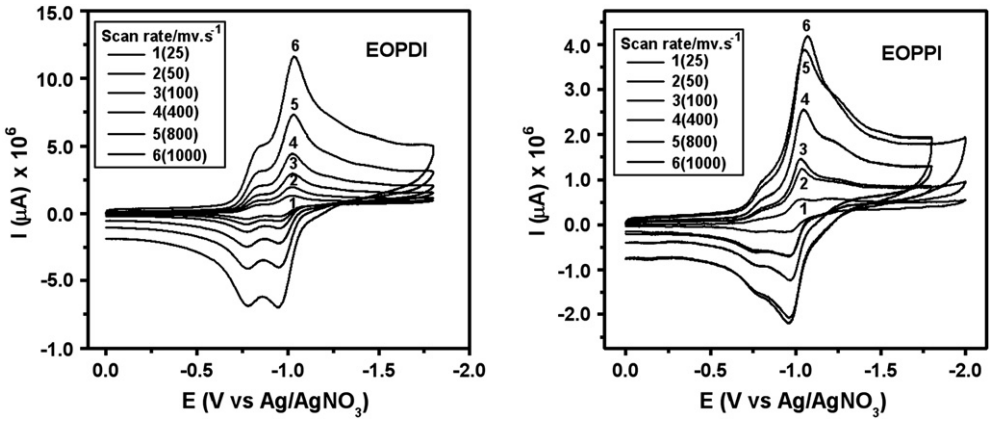

Fig. 11. Cyclic voltammograms of EOPDI and EOPPI (in CH_2Cl_2/supporting electrolyte: $TBAPF_6$, scan rate (mv s^{-1}): 1(25), 2(50), 3(100), 4(400), 5(800), 6(1000)) at 25 °C.

calculated fits was judged using statistical parameters, the reduced χ^2 value and the residual data. As shown in Table 3, the fluorescence quantum yields, oscillator strengths, radiative lifetimes, fluorescence lifetimes, fluorescence rate constants, rate constant of radiationless deactivation and singlet energies data of all the compounds in chloroform were similar but absorption coefficient for the oligomer is found to be enhanced. The calculated and measured fluorescence lifetimes of perylene model compound and oligomer were very similar.

3.3. Thermal stability

The thermal behavior of the monomeric model compound and oligomer was evaluated by thermogravimetry (TGA, heating rate 10 K min^{-1}) and differential scanning calorimetry (second heating scan of DSC, heating rate 10 K min^{-1}) (Fig. 9). The weight loss starting temperatures for some similar polymers were reported around 250 °C [32]. On the other hand, thermal properties of other similar polymers were not given [30–33]. The lower decomposition temperature comparing to the rigid perylene polymers could be attributed to the presence of flexible spacers in the polymer chain that tend to decrease the energy of internal rotation.

EOPDI and EOPPI exhibit no glass transition temperature in the DSC runs (1st and 2nd heating) up to 300 °C. Thermogravimetric analysis of the oligomer showed higher thermal stability comparing to the model compound. The weight loss starting temperature of the model compound and oligomer were 300 and 375 °C, respectively. The temperature of 30% weight loss was 500 °C for the model compound. Additionally, the temperature of 19% weight loss was 600 °C for the oligomeric dye. EOPPI oligomer showed much higher thermal stability than those containing the similar flexible molecular spacers [32]. Accordingly, the oligomeric diimide dye showed higher thermal stability than the model compound that could be attributed to the intermolecular forces, flexibility and symmetry of the structure.

3.4. Electrochemistry

The electrochemical properties of EOPDI and EOPPI were investigated using cyclic (CV) and square-wave (SWV) voltammetries (Figs. 10 and 11) in freshly distilled dichloromethane containing 0.1 M $TBAPF_6$ as a supporting electrolyte and summarized in Tables 4 and 5. All the measured redox potentials, HOMO (highest occupied molecular orbital)/LUMO (lowest unoccupied molecular orbital) and energy gap E_g values obtained from those are tabulated in Table 4. Both model compound and oligomer undergo two reversible one-electron reductions, the first of which is the reduction of the neutral compound to radical anion ($EOPDI^-$ and $EOPPI^-$) and the second reduction corresponds to the formation of the dianion ($EOPDI^{2-}$ and $EOPPI^{2-}$).

EOPDI and EOPPI display reduction processes in their cyclic and square-wave voltammetry (Figs. 10 and 11). Tables 4 and 5 summarize the electrochemical parameters obtained. EOPDI has shown two fast reversible, one-electron reductions at −0.811 and −0.991 V (vs. $Ag/AgNO_3$) with peak potential separations $\Delta E_{p1} = 73$ mV and $\Delta E_{p2} = 71$ mV, respectively, in CH_2Cl_2. Similarly, EOPPI has shown two fast reversible, one-electron reductions at −0.771 and −0.992 V (vs. $Ag/AgNO_3$) with a $\Delta E_{p1} = 59$ mV and $\Delta E_{p2} = 66$ mV, respectively, in CH_2Cl_2. The calculated ΔE_p in the range 60–70 mV for EOPDI and EOPPI shows that reversibility of electron transfer was fairly well maintained in this system.

In order to calculate the absolute energies of LUMO levels of EOPDI and EOPPI with respect to the vacuum level, the redox data are standardized to the ferrocene/ferricenium couple which has a calculated absolute energy of −4.8 eV [38,39]. The LUMO energies of the compounds were calculated from cyclic and square-wave voltammograms (Figs. 10 and 11 and Tables 4 and 5) as −3.78 and −3.85 eV, respectively. The optical band gaps, E_g values, were calculated approximately 2.25 and 2.24 eV for the compounds, respectively, where E_g was obtained from the edge of the electronic absorption band with E_g (eV) $= hc/\lambda$ ($h = 6.626 \times 10^{-34}$ J s, $c = 3 \times 10^{17}$ nm s^{-1}, 1 eV $= 1.602 \times 10^{-19}$ J). From these values, the HOMO energies of the model compound and oligomer were estimated from the relationship $E_{HOMO} = E_{LUMO} - E_g$, as −6.03 and −6.09 eV, respectively.

The electrochemical stability and reversibility of the redox processes of EOPDI and EOPPI were examined using cyclic voltammetry (Fig. 11 and Table 5). Electrochemical stability of the compounds

Table 4
Electrochemical[a] data of EOPDI and EOPPI

	E_{pc} (V)	E_{pa} (V)	ΔE_p (mV)	$E_{1/2}$ vs. $Ag/AgNO_3$ (V)	E_{Fc} vs. $Ag/AgNO_3$ (V)	$E_{1/2}$ vs. Fc (V)	LUMO (eV)	E_g (eV)	HOMO (eV)
EOPDI	−0.774	−0.847	73	−0.811	0.209	−1.020	−3.78	2.25	−6.03
(CH_2Cl_2)	−0.955	−1.026	71	−0.991	0.209	−1.200			
EOPPI	−0.741	−0.800	59	−0.771	0.175	−0.946	−3.85	2.24	−6.09
(CH_2Cl_2)	−0.959	−1.025	66	−0.992	0.175	−1.167			

[a] E_{pc}: cathodic potential, E_{pa}: anodic potential, ΔE_p: peak potential separations, $E_{1/2}$: half wave potential, $Ag/AgNO_3$: silver/silver nitrate reference electrode, E_{Fc}: oxidation potential of ferrocene (internal reference), LUMO: lowest unoccupied molecular orbital, HOMO: highest occupied molecular orbital, E_g: energy gap.

Table 5
Cyclic[a] voltammetry data of EOPDI and EOPPI at different scan rates

Scan rate ($mV\,s^{-1}$)	EOPDI						EOPPI					
	E_{pa} (V)	E_{pc} (V)	ΔE_p (mV)	i_{pa} (μA)	i_{pc} (μA)	i_{pa}/i_{pc} (μA)	E_{pa} (V)	E_{pc} (V)	ΔE_p (mV)	i_{pa} (μA)	i_{pc} (μA)	i_{pa}/i_{pc} (μA)
25	−0.845	−0.774	71	0.60	0.60	1.00	−0.810	−0.741	69	0.20	0.20	1.00
	−1.021	−0.945	76				−1.039	−0.937	102			
50	−0.845	−0.774	71	1.08	1.10	0.98	−0.810	−0.745	65	0.64	0.62	1.03
	−1.022	−0.946	76				−1.035	−0.958	77			
100	−0.847	−0.774	73	1.65	1.61	1.02	−0.800	−0.741	59	0.68	0.63	1.08
	−1.026	−0.955	71				−1.025	−0.959	66			
400	−0.840	−0.774	66	2.28	2.17	1.05	−0.805	−0.747	58	1.43	1.42	1.01
	−1.025	−0.951	74				−1.047	−0.963	84			
800	−0.845	−0.774	71	4.03	3.70	1.09	−0.808	−0.746	62	2.18	2.18	1.00
	−1.029	−0.951	78				−1.050	−0.957	93			
1000	−0.840	−0.779	61	6.17	5.19	1.19	−0.755	−0.812	57	2.33	2.33	1.00
	−1.034	−0.947	87				−1.068	−0.959	109			

[a] In CH_2Cl_2/supporting electrolyte: 0.1 M tetrabutylammonium hexafluorophosphate ($TBAPF_6$), E_{pa}: anodic potential, E_{pc}: cathodic potential, ΔE_p: peak potential separations, i_{pa}: anodic current, i_{pc}: cathodic current.

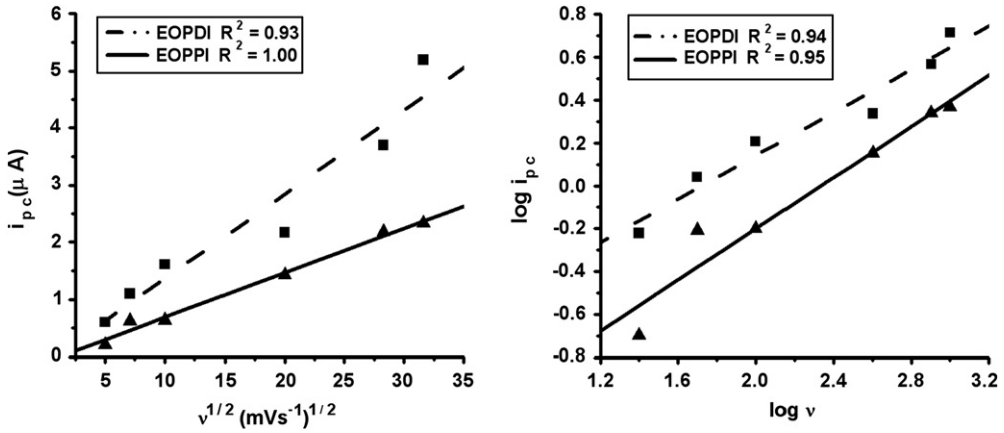

Fig. 12. Effect of variation of scan rates on the peak currents, plot of log ν vs. log i_{pc} of EOPDI and EOPPI (in CH_2Cl_2/supporting electrolyte: $TBAPF_6$).

was examined by measuring repeated cycles of redox processes. EOPDI and EOPPI showed completely reversible reduction steps for the entire scanning rate in a region of 25–1000 $mV\,s^{-1}$. The oligomer has shown similar reduction behavior with the model compound. As seen in Table 5, the calculated peak current ratio, i_{pa} (anodic current)/i_{pc} (cathodic current) was equal to unity and the ΔE_p was about 60–70 mV for each cycle. According to standard reversibility criteria, each reduction process indicates reversible, diffusion-controlled one-electron transfer (Table 5).

A plot of peak current, against square root of scan rate was found to be linear as shown in Fig. 12 ($R^2 = 0.93$ (EOPDI) and 1.00 (EOPPI)), which fulfills the conditions for diffusion-controlled processes. Similarly, the plot of log i_{pc} against log of scan rate (Fig. 12) showed a linear relationship ($R^2 = 0.94$ (EOPDI) and 0.95 (EOPPI)) with a slope of 0.50 (EOPDI, EOPPI), which further confirms the diffusion-controlled nature of the reduction processes.

All electrochemical data are consistent with the $EOPDI^-$/$EOPPI^-$ and $EOPDI^{2-}$/$EOPPI^{2-}$ reduction processes being electrochemically and chemically stable and reversible.

4. Conclusion

In conclusion, a novel soluble oligomeric diimide dye containing alternating perylene and hexa(ethylene glycol) units in the backbone was designed and successfully synthesized by one-step polycondensation. For comparison, its monomeric model compound has been synthesized by the same method. Due to the existence of flexible hydrophilic spacers within the backbone, the diimide oligomer possessed substantial solubility in a wide range of organic solvents such as $CHCl_3$, NMP, DMF and DMSO and so on. On the other hand, alternating rigid hydrophobic perylene tetracarboxylic diimide unit and flexible hydrophilic spacer within the backbone might lead to folding. The oligomer shows very good solubility, much higher thermal stability than those containing the similar flexible molecular spacers and exhibits colors from yellow to red. The thermal stability and concentration-dependent color tunability of the oligomeric diimide is attributed to the existence of the folding within the oligomer. Self-organization might provide an efficient path for charge transfer. The overall results proved that the oligomeric diimide is suitable and remain a challenge for photonics, electronics and sensor applications. Improving the self-organization to obtain an efficient path for charge and energy transport could lead us to an important goal of achieving clean and cheaper energy for the benefit of people.

Acknowledgments

The authors acknowledge the financial support of the Scientific Research Council of Turkey under contract no. TBAG–2371 (103T161). We also thank Dr. Peter Montag in Polymer Standards Service for the GPC measurements.

References

[1] Dotcheva D, Klapper M, Mullen K. Soluble polyimides containing perylene units. Macromol Chem Phys 1994;195(6):1905–11.
[2] Ghassemi H, Zhu JH. Fluorescence of perylene- and naphthalene-containing polyimides: evidence of molecular aggregation and chain coiling in chloroform solution. J Polym Sci B Polym Phys 1995;33(11):1633–9.
[3] Michot C, Baril D, Armand M. Polyimide–polyether mixed conductors as switchable materials for electrochromic devices. Sol Energy Mater Sol Cell 1995;39(2–4):289–99.
[4] Icil H, Icli S. Synthesis and properties of a new photostable polymer: perylene-3,4,9,10-tetracarboxylic acid-bis-(*N*,*N*'-dodecylpolyimide). J Polym Sci A Polym Chem 1997;35(11):2137–42.
[5] Rusanov AL, Elshina LB, Bulycheva EG, Mullen K. Advances in the synthesis of poly(perylenecarboximides) and poly(naphthalenecarboximides). Polym Sci A 1999;41(1):2–21.
[6] Cormier RA, Gregg BA. Synthesis and characterization of liquid crystalline perylene diimides. Chem Mater 1998;10(5):1309–19.
[7] Wang ZY, Qi Y, Gao JP, Sacripante GG, Sundararajan PR, Duff JD. Synthesis, characterization, and xerographic electrical characteristics of perylene-containing polyimides. Macromolecules 1998;31(7):2075–9.
[8] Gregg BA, Cormier RA. Liquid crystal perylene diimide films characterized by electrochemical, spectroelectrochemical, and conductivity versus potential measurements. J Phys Chem B 1998;102(49):9952–7.
[9] Bevers S, O' Dea TP, McLaughlin LW. Perylene- and naphthalene-based linkers for duplex and triplex stabilization. J Am Chem Soc 1998;120(42):11004–5.
[10] Hua J, Meng F, Ding F, Li F, Tian H. Novel soluble and thermally-stable fullerene dyad containing perylene. J Mater Chem 2004;14:1849–53.
[11] Yao D, Bender TP, Gerroir PJ, Sundararajan PR. Self-assembled vesicular nanostructures of perylene end-capped poly(dimethylsiloxane). Macromolecules 2005;38(16):6972–8.
[12] Yao D, Tuteja B, Sundararajan PR. Pigment-mediated nanoweb morphology of poly(dimethylsiloxane)-substituted perylene bisimides. Macromolecules 2006;39(23):7786–8.
[13] Pan J, Zhu W, Li S, Zeng W, Cao Y, Tian H. Dendron-functionalized perylene diimides with carrier-transporting ability for red luminescent materials. Polymer 2005;46(18):7658–69.
[14] Shim JJ, Lee CW, Gong MS. Chemiluminescent properties of perylene-containing polymeric red fluorophores. Synthetic Met 2001;124(2–3):435–41.
[15] Kim DW, Lee CW, Joo SW, Gong MS. Chemiluminescent properties of polyurethane fluorophores containing red and blue chromophore moieties. J Lumin 2002;99(3):205–12.
[16] Park JS, Lee CW, Gong MS. Preparation and chemiluminescent properties of perylene-containing polyimides as polymeric red fluorophores. Synthetic Met 2003;132(2):177–84.
[17] Lee CW, Joo SW, Kim O, Ko J, Gong MS. Synthesis and properties of violet light-emitting polymeric fluorophore. Dyes Pigments 2002;52(1):37–45.
[18] Xu SG, Yang M, Bai F. Novel polyimide containing fluorine and perylene units in the backbone. J Mater Sci Lett 2002;21(24):1903–5.
[19] Klok HA, Becker S, Schuch F, Pakula T, Müllen K. Synthesis and solid state properties of novel fluorescent polyester star polymers. Macromol Biosci 2003;3(12):729–41.
[20] Li C, Pan XG, Hua CF, Su JH, Tian H. Synthesis of novel copoly(styrene-maleic anhydride) materials and their luminescent properties. Eur Polym J 2003;39(6):1091–7.
[21] Huang W, Yan D, Lu QG, Huang Y. Synthesis and characterization of highly soluble fluorescent main chain copolyimides containing perylene units. Eur Polym J 2003;39(6):1099–104.
[22] Yang M, Xu SG, Wan JP, Ye H, Liu X. Synthesis, characterization, and electroluminescent properties of a novel perylene-containing copolyimide. J Appl Polym Sci 2003;90(3):786–91.
[23] Niu H, Wang C, Bai XD, Huang Y. New perylene polyimides containing p–n diblocks for sensitization in TiO_2 solar cells. Polym Adv Tech 2004;15(12):701–7.
[24] Lee CH, Ryu SH, Jang HD, Oh SY. Structural effects of a light emitting copolymer having perylene moieties in the side chain on the electroluminescent characteristics. Mater Sci Eng C 2004;24(1–2):87–90.
[25] Niu H, Wang C, Bai XD, Huang Y. High photoconductivity properties of perylene polyimide containing triarylamine unit. J Mater Sci 2004;39(12):4053–6.
[26] Ha J, Vacha M, Khanchaitit P, Ath-Ong D, Lee SH, Ogino K, et al. Synthesis and characterization of novel light-emitting copolymers containing triphenylamine derivatives. Synthetic Met 2004;144(2):151–8.
[27] Feng L, Chen Z. Synthesis and photoluminescent properties of polymer containing perylene and fluorene units. Polymer 2005;46(11):3952–6.
[28] Xu S, Yang M, Cao S. A fluorescent copolyimide containing perylene, fluorine and oxadiazole units in the main chain. React Funct Polym 2006;66(4):471–8.
[29] Datar A, Balakrishnan K, Yang X, Zuo X, Huang J, Oitker R, et al. Linearly polarized emission of an organic semiconductor nanobelt. J Phys Chem B 2006;110(25):12327–32.
[30] Williams ME, Murray WR. Perylene polyether hybrids: highly soluble, luminescent, redox-active dyes. Chem Mater 1998;10(11):3603–10.
[31] Neuteboom EE, Janssen RAJ, Meijer EW. Aggregation of perylenebisimid-polytetrahydrofuran copolymers. Synthetic Met 2001;121(1–3):1283–4.
[32] Neuteboom EE, Meskers SCJ, Meijer EW, Janssen RAJ. Photoluminescence of self-organized perylene bisimide polymers. Macromol Chem Phys 2004;205(2):217–22.
[33] Li ADQ, Wang W, Wang LQ. Folding versus self-assembling. Chem Eur J 2003;9(19):4594–601.
[34] Ko HC, Lim DK, Kim SH, Choi WG, Lee H. Light-emitting electrochemical cells based on polyimide containing perylene and tri(ethylene oxide) moieties. Synthetic Met 2004;144(2):171–8.
[35] Meng YZ, Hill AR, Hay AS. Poly(imidoaryl ether)s with bulky highly fluorescent pendent groups. Polym Adv Tech 2001;12(3–4):206–14.
[36] He XR, Liu HB, Wang N, Ai XC, Wang S, Li YL, et al. Synthesis and characterization of new types of perylene bisimide-containing conjugated copolymers. Macromol Rapid Comm 2005;26(9):721–7.
[37] Zhou QZ, Jia MX, Shao XB, Wu LZ, Jiang XK, Li ZT, et al. Self-assembly of a novel series of hetero-duplexes driven by donor–acceptor interaction. Tetrahedron 2005;61(30):7117–24.
[38] Peng Z, Bao Z, Galvin ME. Polymers with bipolar carrier transport abilities for light emitting diodes. Chem Mater 1998;10(8):2086–90.
[39] Bredas JL, Silbey R, Bourdreaux DS, Chance RR. Chain-length dependence of electronic and electrochemical properties of conjugated systems: polyacetylene, polyphenylene, polythiophene, and polypyrrole. J Am Chem Soc 1983;105(22):6555–9.